

Maximum Likelihood Estimation for Scaled Inhomogeneous Phase-Type Distributions from Discrete Observations

Fernando Baltazar-Larios*

Facultad de Ciencias

Universidad Nacional Autónoma de México

CdMx, México, A.P. 20-726, 01000

ORCID 0000-0001-8292-3615

fernandobaltazar@ciencias.unam.mx

Alejandra Quintos^{†‡}

Department of Statistics

University of Wisconsin-Madison

Madison, WI, USA, 53706

ORCID 0000-0003-3447-3255

alejandra.quintos@wisc.edu

December 19, 2025

Abstract

Inhomogeneous phase-type (IPH) distributions extend classical phase-type models by allowing transition intensities to vary over time, offering greater flexibility for modeling heavy-tailed or time-dependent absorption phenomena. We focus on the subclass of IPH distributions with time-scaled sub-intensity matrices of the form $\mathbf{\Lambda}(t) = h_\beta(t)\mathbf{\Lambda}$, which admits a time transformation to a homogeneous Markov jump process. For this class, we develop a statistical inference framework for discretely observed trajectories that combines Markov-bridge reconstruction with a stochastic EM algorithm and a gradient-based update. The resulting method yields joint maximum-likelihood estimates of both the baseline sub-intensity matrix $\mathbf{\Lambda}$ and the time-scaling parameter β . Through simulation studies for the matrix-Gompertz and matrix-Weibull families, and a real-data application to coronary allograft vasculopathy progression, we demonstrate that the proposed approach provides an accurate and computationally tractable tool for fitting time-scaled IPH models to irregular multi-state data.

Keywords: Inhomogeneous phase-type distributions; Inhomogeneous Markov jump processes; Stochastic EM algorithm; Time transformation; Markov bridges; Multi-state survival data.

*Supported by UNAM-DGAPA-PAPIIT-IN110926

[†]Supported in part by the Office of the Vice Chancellor for Research and Graduate Education at the University of Wisconsin-Madison with funding from the Wisconsin Alumni Research Foundation

[‡]Corresponding author

1 Introduction

Phase-type (PH) distributions describe the time until absorption of a finite-state homogeneous Markov jump process (MJP) and form a flexible class of distributions with rich structural and analytical properties (see [18]). Inhomogeneous phase-type (IPH) distributions, introduced in [3], extend this framework by defining the absorption time of a finite-state inhomogeneous Markov jump process (IMJP), where transition intensities vary over time. This added flexibility enables IPH distributions to capture phenomena such as heavy-tailed behaviour, non-constant hazard rates, and time-varying transition dynamics that cannot be represented within the homogeneous PH family. Many classical heavy-tailed distributions (including Pareto, Weibull, and generalized extreme value) can be expressed as the distribution of a time-transformed exponential random variable, situating them naturally within the IPH framework.

IPH models have seen increasing use across a wide range of applied domains, including survival analysis [13], queueing systems [23], finance [12], insurance [1], and epidemiology [7]. Despite their flexibility, statistical inference for general IPH distributions is challenging: the time-dependent infinitesimal generator rarely admits closed-form transition probabilities, and the intensity matrices at different time points typically do not commute. These issues complicate likelihood evaluation and make parameter estimation difficult.

A notable subclass of IPH distributions alleviates these challenges by assuming that the sub-intensity matrix can be written in the time-scaled form

$$\mathbf{\Lambda}(t) = h_\beta(t)\mathbf{\Lambda},$$

where h_β is a nonnegative scaling function. This structure ensures that the intensity matrices commute and that the underlying inhomogeneous process can be mapped, via a time transformation, to a homogeneous Markov jump process. The resulting tractability has motivated several recent estimation procedures. For example, [4] propose an expectation-maximization (EM) algorithm for datasets where absorption times are fully observed, and [2] study piecewise-constant models for the time-dependent intensity matrix.

In many practical settings, however, the process is not observed continuously: only the states at discrete and irregular time points are available, and the exact transition times between states remain unobserved. This situation naturally arises in multi-state panel data, such as the progression of chronic diseases monitored at periodic clinical visits. In such cases, estimation becomes a missing-data problem in which both transition times and absorption times must be reconstructed or inferred.

In this work, we develop a statistical inference framework for IPH distributions of the time-scaled form $\mathbf{\Lambda}(t) = h_\beta(t)\mathbf{\Lambda}$ when the underlying IMJP is observed only at discrete time points. Our method combines Markov-bridge simulation with a Stochastic Expectation–Maximization (SEM) algorithm to reconstruct latent continuous-time trajectories and obtain maximum-likelihood estimates of the baseline sub-intensity matrix $\mathbf{\Lambda}$ and the time-scaling parameter β . The SEM step is paired with a gradient-based update for β , producing a flexible and computationally efficient estimation procedure applicable to irregularly spaced observations.

We assess the performance of the proposed method through simulation studies for the matrix-Gompertz and matrix-Weibull families, demonstrating accurate parameter recovery across a range of settings. We then apply the method to coronary allograft vasculopathy (CAV) data, a motivating example involving irregular multi-state observations in a medical setting. We further compare the fitted inhomogeneous model with its homogeneous counterpart, highlighting the importance of accounting for time-varying transition intensities in real-world applications.

The remainder of the paper is organized as follows. Section 2 reviews IPH distributions, their main properties, and the subclass considered in this work. Section 3 presents the proposed estimation procedure in detail. Simulation results are given in Section 4, and Section 5 contains the application to the CAV dataset and the comparison with a homogeneous PH model.

2 Inhomogeneous Phase-Type Distributions

Let $\mathbf{X} = \{X_t\}_{0 \leq t \leq T}$ be an IMJP taking values in a finite state space $E = \{1, 2, \dots, n, n+1\}$, where the states $1, \dots, n$ are transient, and the state $n+1$ is the unique absorbing state. This process is defined by

the initial distribution $\boldsymbol{\alpha} = (\boldsymbol{\pi}, 0)$, where $\boldsymbol{\pi} = (\pi_1, \dots, \pi_n)$, and by the infinitesimal generator $\boldsymbol{Q}(t)$, given by

$$\boldsymbol{Q}(t) := \begin{pmatrix} \boldsymbol{\Lambda}(t) & \boldsymbol{\lambda}(t) \\ \mathbf{0}_n & 0 \end{pmatrix},$$

where $\boldsymbol{\Lambda}(t)$ is an $n \times n$ sub-intensity matrix whose entries depend on time, $\boldsymbol{\lambda}(t) = -\boldsymbol{\Lambda}(t)\mathbb{1}_n$ is the exit-rate vector (with $\mathbb{1}_n$ denoting an n -dimensional column vector of ones), and $\mathbf{0}_n$ is the n -dimensional zero row vector.

Definition 2.1. We define the time until absorption of \boldsymbol{X} as

$$\tau := \inf \{t > 0 \mid X_t = n + 1\},$$

and say that τ follows an IPH distribution with parameters $(\boldsymbol{\pi}, \boldsymbol{\Lambda}(t))$, denoted as $\tau \sim \text{IPH}(\boldsymbol{\pi}, \boldsymbol{\Lambda}(t))$.

Let $\boldsymbol{P}(s, t) = \{p_{xy}(s, t)\}_{x, y \in E}$ ($0 < s < t$) denote the transition probability matrix of the process \boldsymbol{X} , where

$$p_{xy}(s, t) = \mathbb{P}(X_t = y \mid X_s = x),$$

which can be expressed in terms of the product integral of the intensity matrix as (see [20])

$$\boldsymbol{P}(s, t) = \prod_s^t (\boldsymbol{I} + \boldsymbol{\Lambda}(u)du),$$

where the product integral is defined as

$$\prod_s^t (\boldsymbol{I} + \boldsymbol{\Lambda}(u)du) := \boldsymbol{I} + \sum_{k=1}^{\infty} \int_s^t \int_s^{u_k} \cdots \int_s^{u_2} \boldsymbol{\Lambda}(u_1) \cdots \boldsymbol{\Lambda}(u_k) du_1 \cdots du_k.$$

The density and distribution functions of τ (see [3]) are given by

$$f_\tau(x) = \boldsymbol{\pi} \prod_0^x (\boldsymbol{I} + \boldsymbol{\Lambda}(u)du) \boldsymbol{\lambda}(x), \quad (1)$$

and

$$F_\tau(x) = 1 - \boldsymbol{\pi} \prod_0^x (\boldsymbol{I} + \boldsymbol{\Lambda}(u)du) \mathbb{1}_n. \quad (2)$$

If the matrices $\boldsymbol{\Lambda}(t)$ commute for all t , then the density (1) simplifies to

$$f_\tau(x) = \boldsymbol{\pi} \exp\left(\int_0^x \boldsymbol{\Lambda}(t)dt\right) \boldsymbol{\lambda}(x),$$

and the distribution function (2) becomes

$$F_\tau(x) = 1 - \boldsymbol{\pi} \exp\left(\int_0^x \boldsymbol{\Lambda}(t)dt\right) \mathbb{1}_n.$$

In particular, we consider the subclass of IPH distributions in which the intensity matrix takes the form

$$\boldsymbol{\Lambda}(t) = h_\beta(t)\boldsymbol{\Lambda},$$

where $h_\beta(t)$ is a known non-negative real-valued function depending on a parameter β , and $\boldsymbol{\Lambda}$ is a non-time-varying $n \times n$ sub-intensity matrix. We denote this subclass as

$$\tau \sim \text{IPH}(\boldsymbol{\pi}, \boldsymbol{\Lambda}, h_\beta).$$

In this case, all matrices commute and there exists a function g_β defined through its inverse function as

$$g_\beta^{-1}(t) = \int_0^t h_\beta(s) ds,$$

such that

$$\tau \stackrel{d}{=} g_\beta(\rho), \quad \text{where } \rho \sim \text{PH}(\boldsymbol{\pi}, \boldsymbol{\Lambda}).$$

If $\tau \sim \text{IPH}(\boldsymbol{\pi}, \boldsymbol{\Lambda}, h_\beta)$, then the density function f is given by

$$f(\tau; \boldsymbol{\pi}, \boldsymbol{\Lambda}, \beta) = h_\beta(\tau) \boldsymbol{\pi} \exp\left(\int_0^\tau h_\beta(t) dt \boldsymbol{\Lambda}\right) \boldsymbol{\lambda}, \quad (3)$$

and the distribution function F is given by

$$F(\tau; \boldsymbol{\pi}, \boldsymbol{\Lambda}, \beta) = 1 - \boldsymbol{\pi} \exp\left(\int_0^\tau h_\beta(t) dt \boldsymbol{\Lambda}\right) \mathbb{1}_n. \quad (4)$$

Moreover, the expected value of τ is

$$\mathbb{E}[\tau] = \boldsymbol{\pi} L_g(-\boldsymbol{\Lambda}) \boldsymbol{\lambda}, \quad (5)$$

where $L_g(s)$ is the Laplace transform¹, which exists for all $s > \max_i \text{Re}(\gamma_i)$, with γ_i denoting the i -th eigenvalue of $\boldsymbol{\Lambda}$.

We denote by $\mathbf{Y} = \{Y_t\}_{0 \leq t \leq T}$ the homogeneous MJP with infinitesimal generator

$$\mathbf{Q} = \begin{pmatrix} \boldsymbol{\Lambda} & \boldsymbol{\lambda} \\ \mathbf{0}_n & 0 \end{pmatrix},$$

where $\boldsymbol{\Lambda} = \{\lambda_{xy}\}_{x,y=1}^n$ is an $n \times n$ sub-intensity matrix and $\boldsymbol{\lambda} = (\lambda_1, \dots, \lambda_n)^T$ is a column vector of dimension n such that $\boldsymbol{\lambda} = -\boldsymbol{\Lambda} \mathbb{1}_n$ with λ_x denoting the exit rate from state $x = 1, \dots, n$. This process shares the same structural parameters $(\boldsymbol{\pi}, \boldsymbol{\Lambda})$ as the IMJP \mathbf{X} , with the key difference that in \mathbf{X} , the sub-intensity matrix is scaled by the time-dependent function $h_\beta(t)$.

3 Statistical Framework for Estimation

3.1 Observation Scheme and Notation

Consider $K \in \mathbb{N}$ independently and identically distributed (i.i.d.) paths of an underlying IMJP \mathbf{X} , associated with the IPH distribution $\tau \sim \text{IPH}(\boldsymbol{\pi}, \boldsymbol{\Lambda}, h_\beta)$, defined over the time interval $[0, T]$, where $T > 0$. These paths are not observed continuously over time. Instead, for each path $k = 1, \dots, K$, we observe it only at a discrete set of time points denoted by

$$\mathbf{T}^{(k)} := \{0 = t_{k,0} < t_{k,1} < \dots < t_{k,m_k} \leq T\},$$

where $m_k \in \mathbb{N}$ indicates that the k -th path is observed at $m_k + 1$ time points, from $t_{k,0} = 0$ to $t_{k,m_k} \leq T$.

Let \mathbf{X}^d denote the observed discrete-time trajectories:

$$\mathbf{X}^d := \left\{ X_{t_{k,0}} = x_{t_{k,0}}, X_{t_{k,1}} = x_{t_{k,1}}, \dots, X_{t_{k,m_k}} = x_{t_{k,m_k}} \right\}_{k=1}^K,$$

where each $x_{t_{k,j}} \in E$. For instance, $x_{t_{k,0}}$ is the initial state of the k -th path, and $x_{t_{k,m_k}}$ is its last observed state.

Remark 3.1. *Paths are only observed until absorption or censoring. For each k , we allow $t_{k,m_k} \leq T$, meaning that not all paths are necessarily observed up to the terminal time T . Additionally, the absorbing state $n + 1$, if observed, can only occur at the final observation point; that is, $X_{t_{k,j}} \neq n + 1$ for all $j < m_k$, and $X_{t_{k,m_k}}$ may or may not equal $n + 1$.*

¹ $L_g(s) = \int_0^\infty g(t) e^{-st} dt.$

Our objective is to estimate the parameters $(\boldsymbol{\pi}, \boldsymbol{\Lambda}, \beta)^2$. In what follows, we describe the estimation procedure in detail. A summarized version is presented at the end of this section as Algorithm 2.

Remark 3.2. In [4], the parameters $(\boldsymbol{\pi}, \boldsymbol{\Lambda}, \beta)$ were estimated using the EM algorithm under the assumption that the data consist of absorption times observed explicitly. In contrast, our setting considers discretely observed trajectories, where absorption times are generally unobserved and must be inferred indirectly.

Since the initial state of each of the K paths is known, estimation of $\boldsymbol{\pi}$ is straightforward via the empirical distribution. Specifically, let $\hat{\pi}_x$ denote the proportion of paths that start in state $x \in \{1, 2, \dots, n\}$, i.e.,

$$\hat{\pi}_x := \frac{1}{K} \sum_{k=1}^K \mathbb{I}\{x_{t_{k,0}} = x\}, \quad (6)$$

then the estimator is given by

$$\hat{\boldsymbol{\pi}} := (\hat{\pi}_1, \hat{\pi}_2, \dots, \hat{\pi}_n). \quad (7)$$

Estimation of $\boldsymbol{\Lambda}$ and β is performed iteratively and simultaneously by applying a time transformation that converts each inhomogeneous path into an equivalent homogeneous one. Specifically, if t represents a time point in the inhomogeneous scale, then as shown, for example, in [16], the corresponding homogeneous time s is given by

$$s = g_\beta^{-1}(t). \quad (8)$$

Define the time-transformed discrete observations

$$\mathbf{Y}^d := \left\{ Y_{s_{k,0}} = y_{s_{k,0}} = x_{t_{k,0}}, Y_{s_{k,1}} = y_{s_{k,1}} = x_{t_{k,1}}, \dots, Y_{s_{k,m_k}} = y_{s_{k,m_k}} = x_{t_{k,m_k}} \right\}_{k=1}^K,$$

where $s_{k,j} = g_\beta^{-1}(t_{k,j})$ for $j = 0, \dots, m_k$ and $k = 1, \dots, K$. Here, \mathbf{Y}^d represents the discrete observations of a homogeneous MJP \mathbf{Y} associated with the IMJP \mathbf{X} . Furthermore, the associated distribution of \mathbf{Y} is the standard phase-type distribution $\rho \sim \text{PH}(\boldsymbol{\pi}, \boldsymbol{\Lambda})$.

3.2 Methodological Preliminaries

Before presenting our estimation algorithm, we review two simplified estimation scenarios that have been studied in the literature, each assuming that one of the parameters is known and that the underlying process is observed continuously. In these idealized settings, all transition times and visited states are observed exactly. Although our actual data are only observed at discrete time points, these cases serve as building blocks for the more realistic problem of jointly estimating $\boldsymbol{\Lambda}$ and β from discretely observed paths. The two cases are:

- β is known and only $\boldsymbol{\Lambda}$ needs to be estimated (see [8]).
- $\boldsymbol{\Lambda}$ is known and only β needs to be estimated, either by analytically deriving the MLE or by using numerical optimization methods (see [11]).

For both cases, assume that we have $K \in \mathbb{N}$ i.i.d. sample paths of an underlying IMJP \mathbf{X} associated with the IPH distribution $\tau \sim \text{IPH}(\boldsymbol{\pi}, \boldsymbol{\Lambda}, h_\beta)$, defined on the time interval $[0, T]$, where $T > 0$. As mentioned previously, in contrast to our primary setting, we now assume that the paths are observed continuously in time, that is, for each path $k = 1, \dots, K$, we observe the exact times of the transitions and the associated states. The observed data can then be written as

$$\mathbf{X} := \left\{ X_{\tilde{t}_{k,0}} = x_{\tilde{t}_{k,0}}, X_{\tilde{t}_{k,1}} = x_{\tilde{t}_{k,1}}, \dots, X_{\tilde{t}_{k,n_k}} = x_{\tilde{t}_{k,n_k}} \right\}_{k=1}^K, \quad (9)$$

where $x_{\tilde{t}_{k,j}} \in E$ denotes the state entered at transition time $\tilde{t}_{k,j}$ for $j = 0, \dots, n_k$. For example, $x_{\tilde{t}_{k,0}}$ represents the initial state of the k -th path, $\tilde{t}_{k,1}$ is the time of the first transition to state $x_{\tilde{t}_{k,1}}$, and \tilde{t}_{k,n_k} is the final observed transition time into state $x_{\tilde{t}_{k,n_k}}$. Note that for each $k = 1, \dots, K$, the final transition time satisfies $\tilde{t}_{k,n_k} \leq T$.

²We assume that the functional form of h_β is known up to the parameter β .

Remark 3.3. Note that m_k and n_k are not necessarily equal. The quantity $m_k + 1$ represents the number of discrete observation time points for the k -th path, whereas n_k denotes the number of actual state transitions under continuous observation. Additionally, the transition times $\tilde{t}_{k,j}$ in the continuous setting do not generally coincide with the discrete observation times $t_{k,j}$.

We then describe how to handle the more realistic setting in which paths are only observed at discrete time points. This requires using Markov bridges to simulate continuous-time trajectories that are consistent with discretely observed data, assuming the model parameters are known.

Finally, we present a unified perspective that connects all three components (estimation under known β , estimation under known $\mathbf{\Lambda}$, and handling discretely observed data) under a common EM-like framework. This conceptual unification will serve as a guiding principle for the full estimation procedure presented in Section 3.3.

3.2.1 β is known

If β were known, we could transform all observed inhomogeneous time points in equation (9) to their homogeneous equivalents using the time transformation given by equation (8). This results in the transformed data:

$$\mathbf{Y} := \left\{ Y_{\tilde{s}_{k,0}} = y_{\tilde{s}_{k,0}} = x_{\tilde{t}_{k,0}}, Y_{\tilde{s}_{k,1}} = y_{\tilde{s}_{k,1}} = x_{\tilde{t}_{k,1}}, \dots, Y_{\tilde{s}_{k,n_k}} = y_{\tilde{s}_{k,n_k}} = x_{\tilde{t}_{k,n_k}} \right\}_{k=1}^K,$$

where $\tilde{s}_{k,j} = g_\beta^{-1}(\tilde{t}_{k,j})$ for $j = 0, \dots, n_k$ and $k = 1, \dots, K$.

Let $S := g_\beta^{-1}(T)$ denote the transformed terminal time in the homogeneous timeline. The likelihood function of $\mathbf{\Lambda}$, based on the continuous-time trajectories \mathbf{Y} observed over the interval $[0, S]$, is given by (see, e.g., [8]):

$$L_S^c(\mathbf{\Lambda}) = \prod_{x=1}^n \pi_x^{B_x} \prod_{\substack{x=1 \\ y \neq x}}^n \prod_{y=1}^n \left(\lambda_{xy}^{N_{xy}(S)} e^{-\lambda_{xy} R_x(S)} \right) \prod_{x=1}^n \left(\lambda_x^{N_x(S)} e^{-\lambda_x R_x(S)} \right), \quad (10)$$

where:

- $B_x := \sum_{k=1}^K \mathbb{I}\{y_{\tilde{s}_{k,0}} = x\}$ is the number of paths starting in state x ,
- $N_{xy}(S) := \sum_{k=1}^K N_{xy}^k(S)$ is the total number of jumps from state x to y across all paths (with $N_{xy}^k(S)$ denoting the number of such transitions in the k -th path),
- $N_x(S)$ is the total number of jumps from state x to the absorbing state $n + 1$,
- $R_x(S) := \sum_{k=1}^K R_x^k(S)$ is the total time spent in state x across all paths, with $R_x^k(S)$ denoting the time spent in state x by the k -th path.

All indices x, y range over $\{1, \dots, n\}$ with $x \neq y$.

The corresponding log-likelihood function is:

$$\begin{aligned} \ell_S^c(\mathbf{\Lambda}) &= \sum_{x=1}^n B_x \log(\pi_x) + \sum_{x=1}^n \sum_{\substack{y=1 \\ y \neq x}}^n N_{xy}(S) \log(\lambda_{xy}) - \sum_{x=1}^n \sum_{\substack{y=1 \\ y \neq x}}^n \lambda_{xy} R_x(S) \\ &+ \sum_{x=1}^n N_x(S) \log(\lambda_x) - \sum_{x=1}^n \lambda_x R_x(S). \end{aligned} \quad (11)$$

Using standard calculus tools, the MLEs of $\boldsymbol{\pi}$ and $\mathbf{\Lambda}$ are given by:

$$\hat{\pi}_x = \frac{B_x}{K}, \quad \hat{\lambda}_{xy}(S) = \frac{N_{xy}(S)}{R_x(S)}, \quad \hat{\lambda}_x(S) = \frac{N_x(S)}{R_x(S)},$$

provided that $R_x(S) > 0$ for all $x \in \{1, \dots, n\}$.

We summarize this result in the following proposition.

Proposition 3.1 (Maximum Likelihood Estimators in the Homogeneous Timeline). *Suppose β is known and that the continuous-time sample paths of the time-inhomogeneous Markov jump process \mathbf{X} are fully observed over the interval $[0, T]$. Let \mathbf{Y} denote the time-homogeneous MJP obtained by transforming \mathbf{X} via the change of variable $s = g_\beta^{-1}(t)$. Then, the MLEs for the initial distribution $\boldsymbol{\pi}$ and the generator matrix $\boldsymbol{\Lambda}$, based on the trajectories of \mathbf{Y} observed over the homogeneous time interval $[0, S]$, where $S := g_\beta^{-1}(T)$, are given by:*

$$\hat{\pi}_x = \frac{B_x}{K}, \quad \hat{\lambda}_{xy}(S) = \frac{N_{xy}(S)}{R_x(S)}, \quad \hat{\lambda}_x(S) = \frac{N_x(S)}{R_x(S)}, \quad (12)$$

for all $x, y \in \{1, \dots, n\}$ with $x \neq y$, provided that $R_x(S) > 0$ for all x .

Remark 3.4. *The diagonal elements of the generator matrix, λ_{xx} , are not estimated directly. Instead, they are obtained using the fact that each row of $\boldsymbol{\Lambda}$ must sum to zero. Specifically, for each transient state $x \in \{1, \dots, n\}$,*

$$\hat{\lambda}_{xx}(S) = - \left(\sum_{\substack{y=1 \\ y \neq x}}^n \hat{\lambda}_{xy}(S) + \hat{\lambda}_x(S) \right).$$

This ensures that $\boldsymbol{\Lambda}$ remains a valid generator matrix, where the diagonal elements represent the negative total exit rates from each state.

3.2.2 $\boldsymbol{\Lambda}$ is known

In this subsection, we assume that the generator matrix $\boldsymbol{\Lambda}$ is known, and our goal is to estimate the parameter β that maximizes the joint likelihood of K i.i.d. observations drawn from an IPH distribution (see equation (3)). When a closed-form expression for the MLE is not available, numerical optimization methods are commonly employed. In particular, we use the Gradient Descent (GD) method (see [11]).

Since $\boldsymbol{\pi}$, $\boldsymbol{\Lambda}$, and the functional form of h_β are all assumed known (except for the parameter β), the corresponding joint log-likelihood function is given by:

$$\ell_{(t_1, \dots, t_K)}(\beta) = \sum_{k=1}^K \left\{ \log(h_\beta(t_k)) + \log \left(\boldsymbol{\pi} \exp \left(g_\beta^{-1}(t_k) \boldsymbol{\Lambda} \right) \boldsymbol{\lambda} \right) \right\}, \quad (13)$$

where t_k denotes the observed time to absorption for the k -th path.

Remark 3.5. *In this subsection, we implicitly assume that all K paths are observed until absorption, that is, each trajectory reaches the absorbing state before or at time T . This simplifies the exposition and allows for a clean derivation of the likelihood. In subsequent sections, we discuss how to handle the more general case in which some paths may be censored and not absorbed by T .*

We estimate β by maximizing the log-likelihood via GD, an iterative optimization procedure that updates β in the direction of the gradient. This requires evaluating the gradient of the log-likelihood with respect to β , given by:

$$\frac{\partial}{\partial \beta} \ell_{(t_1, \dots, t_K)}(\beta) = \sum_{k=1}^K \left\{ \frac{\frac{\partial}{\partial \beta} h_\beta(t_k)}{h_\beta(t_k)} + \left(\int_0^{t_k} \frac{\partial}{\partial \beta} h_\beta(s) ds \right) \cdot \frac{\boldsymbol{\pi} \boldsymbol{\Lambda} \exp \left(g_\beta^{-1}(t_k) \boldsymbol{\Lambda} \right) \boldsymbol{\lambda}}{\boldsymbol{\pi} \exp \left(g_\beta^{-1}(t_k) \boldsymbol{\Lambda} \right) \boldsymbol{\lambda}} \right\}. \quad (14)$$

Remark 3.6. *To justify differentiating under the integral sign in $g_\beta^{-1}(t) = \int_0^t h_\beta(s) ds$, we assume that $h_\beta(s)$ is continuously differentiable in β for each $s \in [0, T]$, and that $\frac{\partial}{\partial \beta} h_\beta(s)$ is integrable over $[0, T]$. These regularity conditions justify the interchange via the Leibniz integral rule.*

Given the gradient, the GD algorithm proceeds by iteratively updating β . Starting from an initial guess $\hat{\beta}^{(0)}$, each iteration updates the estimate according to:

$$\hat{\beta}^{(i+1)} = \max \left\{ \beta_{\min}, \hat{\beta}^{(i)} + \eta \cdot \frac{\partial}{\partial \beta} \ell_{(t_1, \dots, t_K)} \left(\hat{\beta}^{(i)} \right) \right\}, \quad (15)$$

where $i \in \mathbb{N}$ denotes the iteration index, and $\eta > 0$ is a fixed learning rate (or step size). We fix the lower bound to $\beta_{\min} > 0$ to ensure that $\hat{\beta}$ remains strictly positive.

The procedure is repeated until convergence, which, in our case, is defined as the first iteration i such that:

$$\left| \ell_{(t_1, \dots, t_K)} \left(\hat{\beta}^{(i)} \right) - \ell_{(t_1, \dots, t_K)} \left(\hat{\beta}^{(i-1)} \right) \right| < e_\ell, \quad (16)$$

for a fixed convergence threshold $e_\ell > 0$.

Remark 3.7. *The lower bound $\beta_{\min} > 0$ in the update rule ensures that the parameter β remains strictly positive throughout the optimization process. In our implementation, we set $\beta_{\min} = 10^{-5}$, which is sufficiently small to avoid biasing the estimate while still preventing degenerate behavior.*

3.2.3 Handling Discrete Times

To apply the continuous-time estimation methods described in sections 3.2.1 and 3.2.2 to the discretely observed data \mathbf{X}^d , we must reconstruct plausible continuous-time trajectories of the underlying IMJP that are consistent with the observed states at the discrete time points.

Assume for now that both Λ and β are known. The first step in this reconstruction is to transform the observed time points $(t_{k,1}, t_{k,2}, \dots, t_{k,m_k})$ to the homogeneous time scale using the transformation $s_{k,j} = g_\beta^{-1}(t_{k,j})$, for $k = 1, \dots, K$ and $j = 1, \dots, m_k$. After simulating the corresponding trajectories in the homogeneous time scale, we map them back to the original inhomogeneous scale via the inverse transformation $\tilde{t}_{k,j} = g_\beta(\tilde{s}_{k,j})$, where each $\tilde{s}_{k,j}$ belongs to the set $\{\tilde{s}_{k,1}, \tilde{s}_{k,2}, \dots, \tilde{s}_{k,m_k}\}$ denoting the simulated transition times of the homogeneous MJP.³

A natural way to simulate such homogeneous MJP paths is to condition on the observed states at the transformed time points. This can be achieved using Markov bridges, which sample the latent transitions between consecutive observation times in the homogeneous time scale. These sampled paths yield reconstructed continuous-time trajectories that are consistent with the observed discrete-time states. We define Markov bridges formally below.

Definition 3.1. *A Markov bridge associated with a homogeneous Markov jump process is the process $\{Y_t\}_{t \in [t_1, t_2]}$ conditioned on $Y_{t_1} = x$ and $Y_{t_2} = y$, where $t_1 < t_2$ and $x, y \in E$. We refer to such a bridge as a (t_1, x, t_2, y) -Markov bridge.*

Accordingly, we simulate sample paths from $(s_{k,j}, y_{s_{k,j}}, s_{k,j+1}, y_{s_{k,j+1}})$ -Markov bridges for each $k = 1, 2, \dots, K$ and $j = 0, 1, \dots, m_k - 1$. Various methods for sampling Markov bridges have been extensively studied in the stochastic process and computational statistics literature. A summary and comparison of the most prominent approaches can be found in [6]. In this work, we focus on the rejection sampling method, which is described in the next algorithm.

³We use the same notation convention discussed in Remark 3.3, distinguishing between observed discrete time points and latent transition times under continuous observation.

Algorithm 1 Sampling Markov Bridges via the Rejection Method

Input: $\mathbf{X}^d = \left\{ x_{t_{k,0}}, x_{t_{k,1}}, \dots, x_{t_{k,m_k}} \right\}_{k=1}^K$, $\mathbf{\Lambda}$, and β .

Output: K inhomogeneous, continuous-time paths $\left\{ x_{\tilde{t}_{k,0}}, x_{\tilde{t}_{k,1}}, \dots, x_{\tilde{t}_{k,n_k}} \right\}_{k=1}^K$.

```
1: for  $k \in \{1, 2, \dots, K\}$  do
2:   Transform observation times to the homogeneous scale:  $s_{k,j} = g_\beta^{-1}(t_{k,j})$  for  $j = 0, \dots, m_k$ .
3:   Define  $\mathbf{Y}_k^d = \left\{ y_{s_{k,0}}, y_{s_{k,1}}, \dots, y_{s_{k,m_k}} \right\}$ .
4:   for  $j \in \{0, 1, \dots, m_k - 1\}$  do
5:     Set initial_state  $\leftarrow y_{s_{k,j}}$ , final_state  $\leftarrow y_{s_{k,j+1}}$ , and simulation_time  $\leftarrow s_{k,j+1} - s_{k,j}$ .
6:     while final_state_simulation  $\neq$  final_state do
7:       Simulate a path of a homogeneous MJP over simulation_time, starting in initial_state, with
       generator  $\mathbf{\Lambda}$ .
8:       Record the simulated transition times  $\tilde{s}_{k,j}$  and corresponding states  $y_{\tilde{s}_{k,j}}$ .
9:       Set final_state_simulation to the last state visited in the simulation.
10:    end while
11:  end for
12:  Transform all simulated times to the inhomogeneous scale:  $\tilde{t}_{k,j} = g_\beta(\tilde{s}_{k,j})$  for  $j = 0, \dots, n_k$ .
13: end for
```

Remark 3.8. *The rejection step in line 6 ensures that only simulated trajectories which terminate in the correct final state are accepted. This guarantees that each segment is a valid sample from the corresponding Markov bridge distribution.*

3.2.4 EM-like Estimation under Discrete Observations

When either $\mathbf{\Lambda}$ or β is fixed, estimation of the remaining parameter based on discretely observed trajectories \mathbf{X}^d can be framed as a missing data problem. The full data consist of continuous-time paths of the underlying homogeneous MJP \mathbf{Y} , which are only partially observed at discrete time points.

Estimating $\mathbf{\Lambda}$ given β : We treat the unobserved state transitions between observation times as missing data. Given a fixed β , we use the Stochastic Expectation-Maximization (SEM) algorithm (see [14]) to iteratively:

- **SE-step:** Simulate full trajectories of \mathbf{Y} from the discretely observed data \mathbf{Y}^d using Markov bridges (see Algorithm 1),
- **M-step:** Maximize the expected complete-data log-likelihood to update $\mathbf{\Lambda}$ using equation (12).

This approach corresponds to an SEM subroutine embedded in the full joint estimation procedure (Algorithm 2).

Estimating β given $\mathbf{\Lambda}$: Here, the missing data correspond to the latent absorption times. We simulate these times from the completed trajectories of \mathbf{Y} , map them to the inhomogeneous time scale, and then estimate β by maximizing the log-likelihood given in Section 3.2.2. This maximization is performed via gradient descent (equation (15)).

In both cases, estimation is carried out by alternating between imputing latent data and optimizing a likelihood conditional on that data, which is the essence of SEM-like procedures.

3.3 Full Estimation Procedure

We now have all the necessary tools to describe our complete estimation algorithm. In the remainder of this section, we outline the initialization, iterative procedure, and termination criterion in detail.

3.3.1 Initialization

We begin by specifying an initial guess for the parameter β , denoted by $\hat{\beta}_0$. While the exact value of $\hat{\beta}_0$ is not critical for the correctness of the algorithm, choosing a value close to the true parameter can significantly improve convergence speed.

As previously mentioned, the algorithm relies on a gradient descent procedure. As such, it requires both a step size $\eta > 0$ and a convergence threshold $e_\ell > 0$ for the improvement in the log-likelihood. These two hyperparameters should be selected with care, as they directly influence both the convergence behavior and computational efficiency of the algorithm.

As part of the initialization, we also construct an initial estimate of the generator matrix, denoted $\hat{\Lambda}_0$. To do this, we temporarily treat the K inhomogeneous and discretely observed trajectories as if they were fully observed (i.e., continuous in time) and governed by a homogeneous process. Under these simplifying assumptions, we apply Proposition 3.1 (without performing a time transformation) and obtain $\hat{\Lambda}_0$ using equation (12). We relabel this initial estimate $\hat{\Lambda}_0$ as $\hat{\Lambda}$, which will serve as the starting point for the iterative procedure. This iterative procedure alternates between completing the latent data and maximizing the likelihood, consistent with the SEM structure described above.

We complete the initialization step by refining our initial guess $\hat{\beta}_0$. To this end, we first identify the paths that reached the absorbing state.⁴ For those paths that are absorbed, we treat them as homogeneous and discretely observed. We then simulate plausible absorption times by sampling Markov bridges (see Algorithm 1) using the generator matrix $\hat{\Lambda}$. Note that the absorption time must fall between the final two observation points, i.e., between t_{k,m_k-1} and t_{k,m_k} .

Finally, to refine the initial estimate $\hat{\beta}_0$ and obtain an improved value $\hat{\beta}$, we apply the gradient descent update defined in equation (15) using $\hat{\Lambda}$, $\hat{\pi}$, η , and e_ℓ . The update is repeated until the convergence criterion specified in equation (16) is met.

3.3.2 Iterative Procedure

The following steps form an SEM-like iterative procedure: each iteration alternates between simulating latent continuous-time paths (SE-step), updating Λ via maximum likelihood (M-step), and refining β by gradient-based maximization. These steps are repeated until the termination criterion described in Section 3.3.3 is satisfied.

We begin by transforming all originally observed inhomogeneous time points $\{t_{k,0}, t_{k,1}, \dots, t_{k,m_k}\}_{k=1}^K$ into their homogeneous counterparts. This is done using the time transformation given in equation (8) with the most recent $\hat{\beta}$, yielding the transformed time points:

$$\left\{ s_{k,0} = g_{\hat{\beta}}^{-1}(t_{k,0}), s_{k,1} = g_{\hat{\beta}}^{-1}(t_{k,1}), \dots, s_{k,m_k} = g_{\hat{\beta}}^{-1}(t_{k,m_k}) \right\}_{k=1}^K.$$

Using these transformed data, we simulate continuous-time trajectories in the homogeneous timeline via Markov bridges, as described in Section 3.2.3 and, more specifically, in Algorithm 1.

In applying Algorithm 1, we skip Step 2 since the time transformation has already been performed, and we also skip Step 12, as we will revert to the original time scale later. The simulated continuous-time data in the homogeneous timeline is denoted by:

$$\left\{ y_{\tilde{s}_{k,0}}, y_{\tilde{s}_{k,1}}, \dots, y_{\tilde{s}_{k,n_k}} \right\}_{k=1}^K,$$

where $\tilde{s}_{k,j}$ denotes the latent state transition times.⁵

Special care must be taken for paths that are not absorbed by time $S = g_{\hat{\beta}}^{-1}(T)$. Suppose path k is such a case. Then the final simulated time \tilde{s}_{k,n_k} satisfies $\tilde{s}_{k,n_k} < s_{k,m_k}$, implying that the last observed data point at s_{k,m_k} is not accounted for in the reconstructed path. To retain this information, we add the observation at the final time point to the simulated trajectory:

$$\left\{ y_{\tilde{s}_{k,0}}, y_{\tilde{s}_{k,1}}, \dots, y_{\tilde{s}_{k,n_k}}, y_{s_{k,m_k}} \right\}.$$

⁴Recall from Remark 3.1 that not all paths are necessarily absorbed.

⁵We continue to use the convention from Remark 3.3 to distinguish between observed discrete times and latent continuous transitions.

Next, for each non-absorbed path, we simulate an absorption time. Specifically, we generate a homogeneous MJP trajectory using the current estimate $\hat{\Lambda}$, starting from the final observed state y_{s_k, m_k} , and continue the simulation until the process reaches the absorbing state. This step ensures that each path, whether originally absorbed or censored, is completed as a full homogeneous trajectory terminating in absorption.

We then update the estimate $\hat{\Lambda}$. To do so, we apply equation (12) from Proposition 3.1 in the homogeneous timeline, using all available simulated continuous-time data. This includes both the reconstructed trajectories between observation points (obtained via Markov bridges) and the extended simulations until absorption for originally non-absorbed paths.

To finalize this iteration, we refine the estimate of $\hat{\beta}$. Specifically, we collect the simulated absorption times (in the homogeneous timeline) for all paths and transform them back to the inhomogeneous time scale using the mapping $t = g_{\hat{\beta}}(s)$, based on the current estimate of $\hat{\beta}$. These inhomogeneous absorption times are then used in the gradient descent procedure defined in equation (15), together with the current estimates of $\hat{\Lambda}$, $\hat{\pi}$, the step size η , and the convergence threshold e_ℓ . This $\hat{\beta}$ update is repeated until the stopping criterion in equation (16) is satisfied.

3.3.3 Termination Criterion

As noted at the end of Section 3.3.2, each iteration of the algorithm may involve multiple updates of the parameter estimate $\hat{\beta}$ before the convergence condition in equation (16) is met. Accordingly, we define the termination criterion as follows: the iterative procedure terminates the first time an iteration requires only a single update of $\hat{\beta}$ to satisfy the convergence criterion.

This stopping rule captures the idea that the estimates have sufficiently stabilized, i.e., the gradient descent procedure for refining $\hat{\beta}$ converges immediately within a single update step, indicating that further iterations are unlikely to produce significant changes.

To bring all components together, the full estimation procedure begins with parameter initialization and proceeds via an iterative SEM-like structure that alternates between simulating continuous paths, refining estimates through likelihood maximization and gradient descent, and transitioning between the inhomogeneous and homogeneous timelines. The complete procedure is summarized below in Algorithm 2.

Algorithm 2 Summary of the Full Estimation Procedure

Input: Discrete-time observations \mathbf{X}^d , initial guess $\hat{\beta}_0$, step size $\eta > 0$, convergence threshold $e_\ell > 0$

Output: Estimated parameters $\hat{\pi}$, $\hat{\Lambda}$, $\hat{\beta}$

- 1: **Initialization:**
 - 2: Estimate initial distribution $\hat{\pi}$ using empirical frequencies (equation (7)).
 - 3: Estimate $\hat{\Lambda}_0$ by treating \mathbf{X}^d as continuous (no time transformation) and applying equation (12).
 - 4: Set $\hat{\Lambda} \leftarrow \hat{\Lambda}_0$.
 - 5: Identify all paths absorbed before time T .
 - 6: **for** each absorbed path **do**
 - 7: Sample latent absorption time using Markov bridges (Algorithm 1) and $\hat{\Lambda}$.
 - 8: **end for**
 - 9: Set $\hat{\beta} \leftarrow \hat{\beta}_0$
 - 10: **repeat**
 - 11: Refine $\hat{\beta}$ via gradient descent (equation (15)) using $\hat{\Lambda}$, $\hat{\pi}$, η , and e_ℓ .
 - 12: **until** convergence criterion (16) is satisfied.
 - 13: **Iterative Estimation:**
 - 14: **repeat**
 - 15: Transform all observed time points to the homogeneous scale using $s = g_{\hat{\beta}}^{-1}(t)$.
 - 16: **for** each path $k = 1, \dots, K$ **do**
 - 17: Simulate latent continuous-time transitions between $s_{k,0}, \dots, s_{k,m_k}$ using Markov bridges (Algorithm 1).
 - 18: **if** path k is not absorbed by time $S = g_{\hat{\beta}}^{-1}(T)$ **then**
 - 19: Add the last observed state $y_{s_{k,m_k}}$ to the simulated trajectory.
 - 20: Simulate absorption time (in homogeneous time) starting from $y_{s_{k,m_k}}$ using $\hat{\Lambda}$.
 - 21: **end if**
 - 22: **end for**
 - 23: Update $\hat{\Lambda}$ via MLE using equation (12) and all simulated homogeneous trajectories.
 - 24: Transform simulated absorption times from homogeneous to inhomogeneous scale using $t_k = g_{\hat{\beta}}(s_k)$.
 - 25: **repeat**
 - 26: Update $\hat{\beta}$ via gradient descent (equation (15)) using $\hat{\Lambda}$, $\hat{\pi}$, η , and e_ℓ .
 - 27: **until** convergence criterion (16) is satisfied
 - 28: **until** an iteration in which $\hat{\beta}$ converges after a single update (see Section 3.3.3)
 - 29: **Return** $\hat{\pi}$, $\hat{\Lambda}$, $\hat{\beta}$
-

Remark 3.9. Given the current estimate of $\hat{\beta}$, Steps 15–23 in Algorithm 2 implement a SEM update for Λ ; under mild regularity conditions, SEM iterations are known to increase the complete-data likelihood on average and to converge in distribution toward a neighborhood of a maximum of the likelihood [21].

Similarly, Steps 25–27 apply gradient descent to the complete-data log-likelihood in β . With an appropriate choice of step size η and convergence threshold e_ℓ , this procedure typically converges to a local maximizer of the complete-data objective [11].

Overall, the algorithm alternates between updating Λ and β in a way that monotonically improves the likelihood of the simulated complete data. In our experiments, this SEM–GD scheme consistently stabilized after a moderate number of iterations, yielding parameter estimates that provided excellent fits to both simulated and real datasets.

4 Simulation Study

In this section, we conduct a simulation study using two scaling functions to evaluate the accuracy of the calibration method proposed in this work.

4.1 Gompertz Distribution

In this case, the scaling function is $h_\beta(t) = e^{\beta t}$, with $\beta > 0$. The function g_β^{-1} associated with this scaling function is given by

$$g_\beta^{-1}(t) = \int_0^t e^{\beta s} ds = \frac{1}{\beta} (e^{\beta t} - 1).$$

Inverting this expression, we obtain

$$g_\beta(s) = \frac{1}{\beta} \log(\beta s + 1).$$

Therefore, the absorption time τ of the inhomogeneous process satisfies

$$\tau = \frac{1}{\beta} \log(\beta \rho + 1),$$

where $\rho \sim \text{PH}(\boldsymbol{\pi}, \boldsymbol{\Lambda})$. The resulting distribution of τ is known as *matrix-Gompertz distribution*. The Gompertz distribution is commonly used to model human lifetimes (see [15]). In [4], the authors use this distribution to model the lifetime of the Danish population.

The distribution function of τ is given by

$$F(\tau; \boldsymbol{\pi}, \boldsymbol{\Lambda}, \beta) = 1 - \boldsymbol{\pi} e^{\boldsymbol{\Lambda}(e^{\beta\tau} - 1)/\beta} \mathbf{1}_n,$$

and the corresponding density function is

$$f(\tau; \boldsymbol{\pi}, \boldsymbol{\Lambda}, \beta) = \boldsymbol{\pi} e^{\boldsymbol{\Lambda}(e^{\beta\tau} - 1)/\beta} \boldsymbol{\lambda} e^{\beta\tau}.$$

Assuming x_1, \dots, x_m are i.i.d. realizations from this distribution, given fixed estimates $\hat{\boldsymbol{\pi}}$ and $\hat{\boldsymbol{\Lambda}}$, the likelihood function of β is

$$L(\beta) = \prod_{i=1}^m \hat{\boldsymbol{\pi}} e^{\hat{\boldsymbol{\Lambda}}(e^{\beta x_i} - 1)/\beta} \hat{\boldsymbol{\lambda}} e^{\beta x_i},$$

then the corresponding log-likelihood function is

$$l(\beta) = \sum_{i=1}^m \log \left[\hat{\boldsymbol{\pi}} e^{\hat{\boldsymbol{\Lambda}}(e^{\beta x_i} - 1)/\beta} \hat{\boldsymbol{\lambda}} e^{\beta x_i} \right],$$

and its derivative with respect to β is

$$l'(\beta) = \sum_{i=1}^m \frac{\hat{\boldsymbol{\pi}} e^{\hat{\boldsymbol{\Lambda}}(e^{\beta x_i} - 1)/\beta} e^{\beta x_i} \left[\frac{\hat{\boldsymbol{\Lambda}} x_i e^{\beta x_i}}{\beta} \hat{\boldsymbol{\lambda}} + \hat{\boldsymbol{\lambda}} x_i - \frac{\hat{\boldsymbol{\Lambda}}(e^{\beta x_i} - 1)}{\beta^2} \hat{\boldsymbol{\lambda}} \right]}{\hat{\boldsymbol{\pi}} e^{\hat{\boldsymbol{\Lambda}}(e^{\beta x_i} - 1)/\beta} \hat{\boldsymbol{\lambda}} e^{\beta x_i}}.$$

To assess the performance of our estimation procedure, we generate $K = 1000$ sample paths from an IMJP \mathbf{X} , defined over the time interval $[0, 60]$, with $n = 3$ transient states. The parameters used to generate the simulated data correspond to the estimators reported in [4]: $\boldsymbol{\pi} = (0.0451, 0.1303, 0.8246)$, $\beta = 0.1019$, and

$$\boldsymbol{\Lambda} = \begin{pmatrix} -0.1357 & 0.1214 & 0.0000 \\ 0.0130 & -0.0421 & 0.0288 \\ 0.1415 & 0.0184 & -0.1620 \end{pmatrix}.$$

The estimation is based on discrete-time observations \mathbf{X}^d (which we treat as the observed data), where for all $i \in \{1, \dots, m_k\}$, and $k \in \{1, \dots, K\}$, the time intervals between observations are given by: $t_{k,i} - t_{k,i-1} = 1$. We apply the full estimation procedure described in Algorithm 2, which jointly estimates the parameters $(\hat{\boldsymbol{\pi}}, \hat{\boldsymbol{\Lambda}}, \hat{\beta})$ from discretely observed sample paths.

The SEM algorithm is initialized, using the method described in Section 3.3.1, with

- The initial value $\hat{\beta}_0 = 1$,

- An initial sub-intensity matrix $\hat{\mathbf{A}}_0$, obtained by applying the maximum likelihood estimator for homogeneous MJPs described in Proposition 3.1, treating the discrete-time observations \mathbf{X}^d as if they were continuously observed paths from a homogeneous process (i.e., no time transformation was applied).

At each iteration, as detailed in 3.3.2, continuous-time sample paths are reconstructed using Markov bridges, followed by maximum likelihood updates for $\hat{\mathbf{A}}$ and a gradient-based refinement of $\hat{\beta}$, specifically using the update rule given in equation (15) with learning rate $\eta = 10^{-6}$ and convergence threshold $e_\ell = 0.01$.

In Table 1, we present the estimated values of the parameters for different time horizons T . Recall that, as defined in Section 3, T represents the total observation time.

Table 1: Estimated Parameters for Different Values of T (Gompertz Model)

T	$\hat{\beta}$	$\hat{\lambda}_{11}$	$\hat{\lambda}_{12}$	$\hat{\lambda}_{13}$	$\hat{\lambda}_{21}$	$\hat{\lambda}_{22}$	$\hat{\lambda}_{23}$	$\hat{\lambda}_{31}$	$\hat{\lambda}_{32}$	$\hat{\lambda}_{33}$
60	0.1025	-0.1381	0.1218	0.0019	0.0131	-0.0420	0.0285	0.1432	0.0165	-0.1620
47	0.1027	-0.1364	0.1199	0.0021	0.0130	-0.0415	0.0279	0.1421	0.0167	-0.1605
39	0.1124	-0.1194	0.1055	0.0013	0.0096	-0.0356	0.0258	0.1346	0.0141	-0.1510
36	0.1426	-0.0796	0.0709	0.0013	0.0063	-0.0236	0.0173	0.0923	0.0123	-0.1051
True Values	0.1019	-0.1357	0.1214	0.0000	0.0130	-0.0421	0.0288	0.1415	0.0184	-0.1620

Since our primary interest is estimating the time-inhomogeneous generator, we omit the estimates of the initial distribution $\boldsymbol{\pi}$. These estimates are not central to our algorithm and, importantly, remain constant across all values of T , as they depend solely on the distribution of initial states at time 0.

Shorter observation windows lead to fewer absorption events in the dataset, limiting the available information and reducing the accuracy of the estimated parameters. This pattern is reflected in Table 2, which reports the number of absorbed paths (out of 1000), the iteration at which the algorithm converged, and a p-value assessing the fit for each value of T . As T decreases, the number of absorbed paths drops, requiring more iterations for convergence and yielding lower p-values.

The p-values are computed using a two-sample Kolmogorov-Smirnov (KS) test, which compares the empirical distribution of absorption times from the observed data with that from the simulated data under the estimated parameters. A larger p-value indicates less evidence against the null hypothesis that the two samples come from the same distribution, whereas a small p-value suggests a poor fit of the estimated model to the observed data.

Table 2: Simulation Results and Goodness-of-Fit for Different Values of T

T	Absorbed Paths	Iteration	p-value
60	1000	31	0.9135
47	983	33	0.828
39	834	42	0.4324
36	747	59	4.015×10^{-5}

When $T = 36$, the observed time covers only about 60% of the full trajectory horizon, leading to a significant loss of absorption information. This loss explains the extremely low p-value in the last row of Table 2, indicating that the estimated distribution diverges substantially from the true one in that setting.

This behavior is further illustrated in Figure 1, which compares the empirical distributions of the observed absorption times (under the true parameters) with those of the simulated absorption times (under the estimated parameters). For large values of T , the agreement between the distributions is strong, confirming the quality of the fit. As T decreases, noticeable discrepancies emerge, consistent with the trend in the p-values. In particular, the empirical distribution of absorption times becomes increasingly left-skewed and compressed, indicating that shorter observation windows not only reduce the number of observed absorption events, but also systematically truncate the right tail of the distribution.

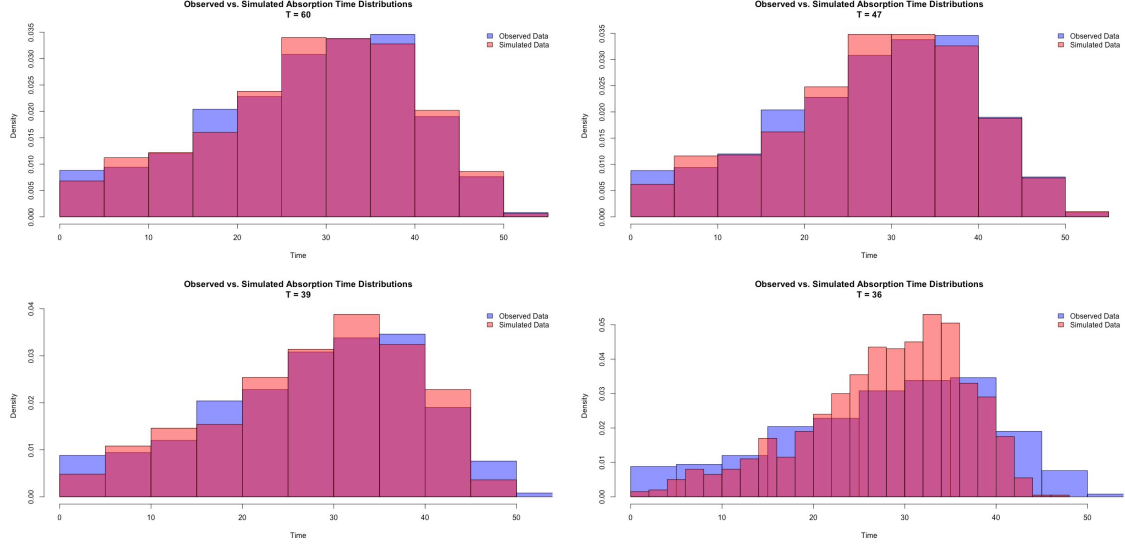


Figure 1: Comparison of absorption time distributions for observed data (\mathbf{X}^d) vs. simulated data (under estimated parameters). Each panel corresponds to a different value of T .

4.2 Matrix Weibull Distribution

In this case, the scaling function is defined as $h_\beta(t) = \beta t^{\beta-1}$, with $\beta > 0$. The associated transformation g_β^{-1} is given by:

$$g_\beta^{-1}(t) = \int_0^t \beta s^{\beta-1} ds = t^\beta,$$

so its inverse is

$$g_\beta(s) = s^{1/\beta}.$$

Therefore, if $\rho \sim \text{PH}(\pi, \Lambda)$, then the absorption time of the inhomogeneous process satisfies

$$\tau = \rho^{1/\beta},$$

and the resulting distribution of τ is referred to as matrix Weibull distribution. It is defined through a matrix transformation of the Weibull cumulative distribution function, enabling flexible modeling of lifetimes and survival data with complex dependence structures and non-monotonic hazard rates (see [10]).

The density and distribution functions of τ are given by:

$$\begin{aligned} F(\tau; \pi, \Lambda, \beta) &= 1 - \pi e^{\Lambda \tau^\beta} \mathbb{1}_n, \\ f(\tau; \pi, \Lambda, \beta) &= \pi e^{\Lambda \tau^\beta} \boldsymbol{\lambda} \cdot \beta \tau^{\beta-1}. \end{aligned}$$

Assume x_1, \dots, x_m are i.i.d. realizations from this distribution. Given fixed estimates $\hat{\boldsymbol{\pi}}$ and $\hat{\boldsymbol{\Lambda}}$, the likelihood function for β is

$$L(\beta) = \prod_{i=1}^m \hat{\boldsymbol{\pi}} e^{\hat{\boldsymbol{\Lambda}} x_i^\beta} \hat{\boldsymbol{\lambda}} \cdot \beta x_i^{\beta-1},$$

and the corresponding log-likelihood function becomes:

$$\ell(\beta) = \sum_{i=1}^m \left[\log \left(\hat{\boldsymbol{\pi}} e^{\hat{\boldsymbol{\Lambda}} x_i^\beta} \hat{\boldsymbol{\lambda}} \right) + \log(\beta) + (\beta - 1) \log(x_i) \right].$$

To assess the performance of the estimation procedure, we generate $K = 1000$ sample paths from an IMJP X on the interval $[0, 5]$ with $n = 2$ transient states. The parameters used are taken from [9]:

$$\pi = (0.5, 0.5), \quad \beta = 3, \quad \Lambda = \begin{pmatrix} -3 & 0.1 \\ 0.01 & -0.1 \end{pmatrix}.$$

For estimation, we observe the process only at discrete times $(t_{k,1}, t_{k,2}, \dots, t_{k,m_k})$ over the interval $[0, 5]$ with $t_{k,i} - t_{k,i-1} = 0.1$ for $k = 1, \dots, K$ and $j = 1, \dots, m_k$. We apply the full estimation procedure described in Algorithm 2, which jointly estimates the parameters $(\hat{\boldsymbol{\pi}}, \hat{\boldsymbol{\Lambda}}, \hat{\beta})$ from discretely observed sample paths.

The SEM algorithm is initialized, using the method described in Section 3.3.1, with:

- An initial value $\hat{\beta}_0 = 2$,
- An initial sub-intensity matrix $\hat{\boldsymbol{\Lambda}}_0$, obtained by applying the maximum likelihood estimator for homogeneous MJPs described in Proposition 3.1, treating the discrete-time observations \mathbf{X}^d as if they were continuously observed paths from a homogeneous process (i.e., no time transformation was applied).

At each iteration, as detailed in Section 3.3.2, continuous-time sample paths are reconstructed using Markov bridges, followed by maximum likelihood updates for $\hat{\boldsymbol{\Lambda}}$ and a gradient-based refinement of $\hat{\beta}$, specifically using the update rule given in equation (15) with learning rate $\eta = 10^{-4}$ and convergence threshold $e_\ell = 0.01$.

Table 3 presents the estimated values of the parameters at iteration 17, which corresponds to the point at which Algorithm 2 reaches convergence. Figure 2 illustrates the evolution of the estimators across the 17 iterations.

The goodness-of-fit of the estimated model is assessed using a two-sample Kolmogorov–Smirnov (KS) test. The resulting p-value is 0.9541, indicating strong agreement between the empirical distribution of absorption times under the estimated parameters and that generated under the true parameters, as described in Section 4.1.

Table 3: Estimated Parameters (Matrix Weibull Model)

Parameter	True Value	Estimator
β	3	2.93065
λ_{11}	-3	-2.86090
λ_{12}	0.1	0.10633
λ_{21}	0.01	0.01329
λ_{22}	-0.1	-0.10115

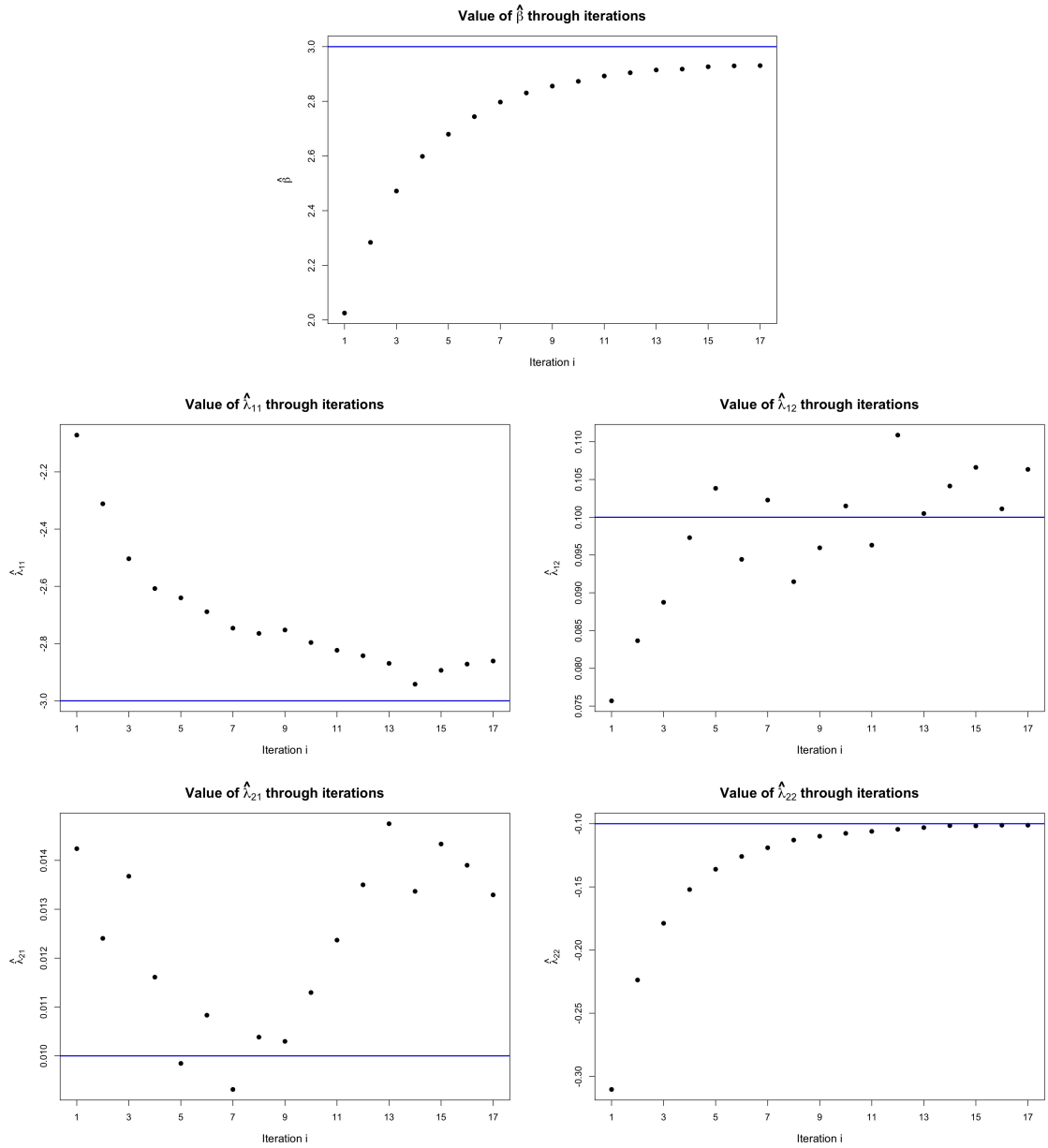


Figure 2: Evolution of the estimators across iterations, converging at iteration 17. The horizontal blue line indicates the true parameter value. Note that the scale of the vertical axis differs across plots.

Figure 3 provides a visual comparison between the theoretical density of the true matrix Weibull distribution (using the parameters given in [9]) and the density obtained using the estimated parameters (from Table 3). The close agreement between the two curves confirms the accuracy of the estimation procedure. The estimated density not only tracks the mode and decay pattern of the true model, but also captures the multi-modal structure introduced by the inhomogeneity.

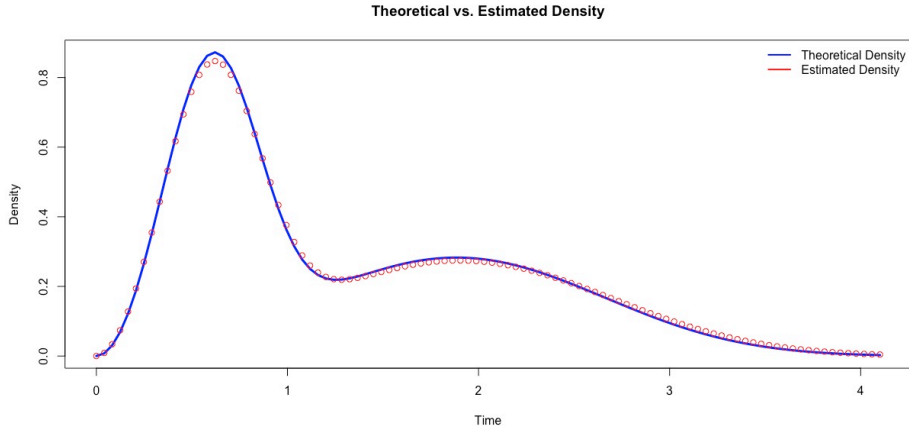


Figure 3: Comparison of the true theoretical density (blue) with the estimated density (red) for the matrix Weibull model.

5 Real Data Application

The dataset comes from monitoring a group of heart transplant recipients, available in the `msm` package in R [17]. It contains records for 622 patients, tracking the progression of coronary allograft vasculopathy (CAV), a post-transplant deterioration of the arterial walls. Each patient underwent periodic angiograms, typically once a year after transplantation, to diagnose and monitor CAV development. Based on the angiogram results, each patient’s condition was classified into one of three possible states: CAV-free, mild CAV, or moderate/severe CAV. A fourth state, death, represents the absorbing state and is recorded at the time of the patient’s death, measured in years since transplantation.

All patients begin in state 1 (CAV-free). Among the 622 records, only 251 patients reached the absorbing state (death). For model fitting, we considered the 251 absorbed records and the 15 non-absorbed records that transitioned through all three transient states: CAV-free, mild CAV, and moderate CAV. Records that did not visit these three states were excluded, as they provide limited information about disease progression. The resulting dataset consists of discrete-time observations of each of the 266 patients’ CAV status at the times of their medical visits. Importantly, the observation times are irregular: the intervals between visits, denoted by $t_{k,i} - t_{k,i-1}$, vary both across and within patients. This irregular sampling poses a challenge for parameter estimation, since the exact transition times between states are unobserved and differ across trajectories; precisely the type of setting for which our proposed SEM-based inference method is designed. We divided the dataset into training and test samples, with 132 and 134 patients, respectively.

A further feature of the dataset is that some patients share exactly the same recorded absorption time (i.e., time of death). We retain these repeated absorption times in our analysis. Even when two individuals die at the same recorded time, their intermediate trajectories may differ substantially—in both the spacing of visits and the sequence of observed CAV states—and both features carry meaningful information for estimating transition intensities. Removing such observations would therefore discard informative patterns in the data. Moreover, because the train–test split is random, repeated absorption times naturally appear in both subsets, further supporting the decision to keep the dataset intact.

The choice of the scaling function $h_\beta(t) = e^{\beta t}$ is motivated by the well-established success of Gompertz-type dynamics in modeling human mortality and other biological aging processes. The Gompertz distribution has long been used to describe lifetimes and failure rates that increase exponentially with time [15], and recent studies have shown that inhomogeneous phase-type distributions provide accurate representations of mortality curves across the entire lifespan [5]. Furthermore, Gompertz-type dynamics naturally arise in interacting failure systems, supporting their application to chronic vascular processes [19]. This distribution has also been widely applied in survival analyses of cancer clinical trials with long-term survivors, illustrating its flexibility in modeling asymmetric hazard trajectories [22]. Collectively, these findings motivate the use of an exponential scaling function to capture the accelerating risk of CAV progression following transplantation.

We ran Algorithm 2 with the scaling function $h_\beta(t) = e^{\beta t}$, initial value $\hat{\beta}_0 = 2$, and initial sub-intensity matrix $\hat{\mathbf{\Lambda}}_0$ obtained by applying the maximum likelihood estimator for homogeneous MJPs described in Proposition 3.1, treating the discrete-time observations \mathbf{X}^d as if they were continuously observed paths from a homogeneous process (i.e., no time transformation was applied). Note that since all patients start in state 1, the initial distribution is fixed as $\hat{\pi} = (1, 0, 0, 0)$. The learning rate was set to $\eta = 0.00001$ and the convergence threshold to $e_\ell = 0.001$. The algorithm reached convergence after 8 iterations, yielding the estimates $\hat{\beta} = 0.0921$ and

$$\hat{\mathbf{\Lambda}} = \begin{pmatrix} -0.2068 & 0.1015 & 0.0130 \\ 0.0833 & -0.3452 & 0.1984 \\ 0.0144 & 0.0217 & -0.1445 \end{pmatrix}.$$

The estimated sub-intensity matrix $\hat{\mathbf{\Lambda}}$ characterizes the baseline transition structure among the three transient states describing CAV progression. Since the inhomogeneous model assumes $\Lambda(t) = e^{\beta t} \Lambda$, the instantaneous transition intensities increase exponentially with time. Thus, the entries of $\hat{\mathbf{\Lambda}}$ reflect the relative strength of transitions, while the overall progression of CAV accelerates with time since transplantation.

The largest off-diagonal elements correspond to the transitions from mild to moderate CAV ($\hat{\lambda}_{23} = 0.1984$) and from CAV-free to mild CAV ($\hat{\lambda}_{12} = 0.1015$), indicating that disease progression typically follows the sequential pathway $1 \rightarrow 2 \rightarrow 3$. Direct transitions between nonadjacent states are comparatively rare, as reflected by the smaller rate $\hat{\lambda}_{13} = 0.0130$. Interestingly, state 2 (mild CAV) is the most transient one: it has the largest total exit rate ($|\hat{\lambda}_{22}| = 0.3452$), indicating that patients spend the least time in state 2. In contrast, state 3 has the smallest total exit rate ($|\hat{\lambda}_{33}| = 0.1445$), implying the longest expected duration in that state. This relative stability may reflect behavioral adaptation: once patients are diagnosed with moderate/severe CAV, they often receive closer monitoring and modify their lifestyle or treatment, slowing further progression.

The absorption (death) rates from each transient state can be computed as the negatives of the row sums of $\hat{\mathbf{\Lambda}}$, i.e., $\hat{\boldsymbol{\lambda}} = -\hat{\mathbf{\Lambda}} \mathbf{1}_3$:

$$\hat{\lambda}_1 = 0.0923, \quad \hat{\lambda}_2 = 0.0635, \quad \hat{\lambda}_3 = 0.1083.$$

These values suggest that patients in the moderate/severe CAV state exhibit the highest instantaneous risk of death, followed by those in the CAV-free state. The relatively smaller absorption rate for the mild CAV state is consistent with the fact that most exits from this state are progressions to moderate/severe CAV rather than death.

To evaluate the accuracy of the estimated parameters and the adequacy of the chosen scaling function $h_\beta(t)$, we used the fitted model to generate simulated data and compared it with the real observations. Specifically, we simulated complete trajectories until absorption (all simulations reached the absorbing state) and compared the resulting absorption times with those observed among the 126 patients in the test sample who reached absorption. The goodness-of-fit was assessed using a two-sample Kolmogorov–Smirnov (KS) test, as in the examples in Section 4. The resulting p-value of 0.3338 indicates strong agreement between the empirical distribution of absorption times generated under the estimated parameters and that observed in the real data. This behavior is further illustrated in Figure 4, which compares the empirical distributions of the observed absorption times with those obtained from the simulated data under the estimated model.

Real vs. Simulated Absorption Time Distributions

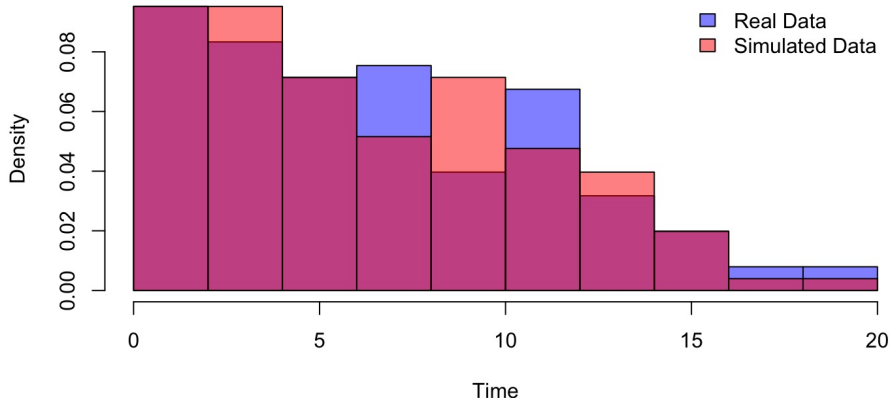


Figure 4: Comparison of the empirical distributions of absorption times for the real (test sample) and simulated data under the estimated parameters. The KS test yields a p-value of 0.3338.

The results obtained from the real dataset confirm the practical relevance of the proposed estimation procedure. The inhomogeneous phase-type model, combined with the scaling function $h_\beta(t) = e^{\beta t}$, provides an accurate description of the progression of CAV over time and captures the increasing risk dynamics associated with disease advancement. Overall, the close agreement between simulated and observed absorption times demonstrates that the proposed method effectively models complex time-dependent transitions in multi-state data.

To assess the importance of accounting for time inhomogeneity, we also fitted a homogeneous phase-type model to the same dataset, assuming constant transition intensities over time. In this case, the intensity matrix $\mathbf{\Lambda}(t)$ was replaced by a time-invariant sub-intensity matrix $\mathbf{\Lambda}$, which was estimated using a simplified version of Algorithm 2. Specifically, the estimation procedure omitted the parameter β and the time transformations governed by the functions g and g^{-1} , which were set to the identity. Since the convergence criterion in Algorithm 2 depends on likelihood updates involving β (see equation (16)), there was no need to specify a learning rate η or a convergence threshold e_ℓ . Instead, we ran the algorithm for 300 iterations to allow sufficient warm-up and obtained the final estimate of $\mathbf{\Lambda}$ as the average of the last 20 iterations. This adaptation ensures comparability with the inhomogeneous case while preserving the stochastic structure of the SEM-based estimation procedure.

As in the inhomogeneous case, we used the fitted homogeneous model to generate simulated trajectories until absorption and compared them with the real observations (using the same train–test split as before). As expected, the homogeneous model provided a noticeably poorer fit: the empirical and simulated absorption time distributions differed substantially, particularly in the tails, as shown in Figure 5. The corresponding KS test yielded a significantly lower p-value of 0.04516, leading to rejection of the null hypothesis that the two samples come from the same distribution.

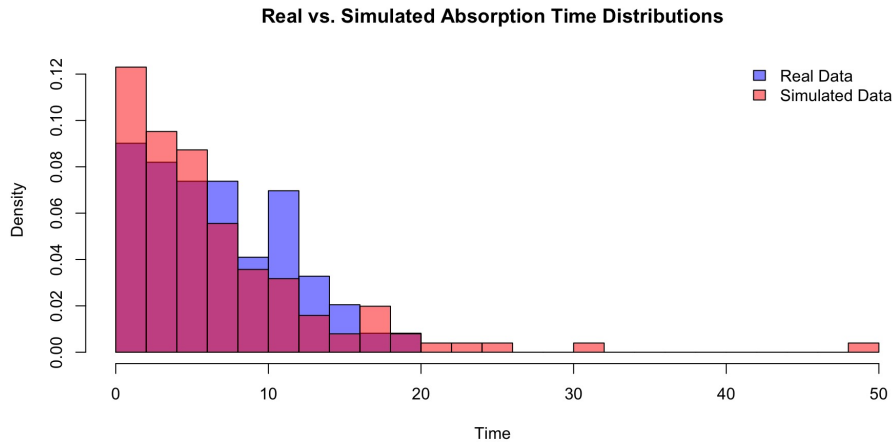


Figure 5: Comparison of the empirical distributions of absorption times for the real (test sample) and simulated data under the estimated parameters assuming homogeneity. The KS test yields a p-value of 0.04516.

This comparative analysis highlights that our SEM-based inference method not only captures the temporal evolution of transition intensities but also yields reliable parameter estimates even under irregular and discretely observed data, establishing a robust foundation for future applications of inhomogeneous phase-type models.

References

- [1] J. Ahmad and M. Bladt, *Phase-type representations of stochastic interest rates with applications to life insurance*, European Actuarial Journal 13 (2023), pp. 571–606. Available at <https://doi.org/10.1007/s13385-023-00346-4>.
- [2] M. Ahmad J. Bladt and M. Bladt, *Estimating absorption time distributions of general markov jump processes.*, Scandinavian Journal of Statistics 51 (2024), pp. 171–200.
- [3] H. Albrecher and M. Bladt, *Inhomogeneous phase-type distributions and heavy tails.*, Journal of Applied Probability 56 (2019), pp. 1044–1064.
- [4] H. Albrecher, M. Bladt, and J. Yslas, *Fitting inhomogeneous phase-type distributions to data: the univariate and the multivariate case.*, Scandinavian Journal of Statistics 29 (2022), pp. 44–77.
- [5] H. Albrecher, M. Bladt, M. Bladt, and J. Yslas, *Mortality modeling and regression with matrix distributions*, Insurance: Mathematics and Economics 107 (2022), pp. 68–87. Available at <https://doi.org/10.1016/j.insmatheco.2022.08.001>.
- [6] F. Baltazar-Larios and L. Judith R. Esparza, *A novel method and comparison of methods for constructing markov bridges*, Computational Statistics (2025), pp. 1–22.
- [7] N.R. Barraza, G. Pena, and V. Moreno, *A non-homogeneous markov early epidemic growth dynamics model. application to the sars-cov-2 pandemic*, Chaos, Solitons & Fractals 139 (2020), p. 110297.
- [8] P. Billingsley, *Statistical Inference for Markov Processes.*, The University of Chicago Press, Chicago., 1961.
- [9] M. Bladt and O. Peralta, *Strongly convergent homogeneous approximations to inhomogeneous markov jump processes and applications*, Mathematics of Operations Research 50 (2025), pp. 334–355. Available at <https://doi.org/10.1287/moor.2022.0153>.

- [10] M. Bladt and L. Rojas-Nandayapa, *The matrix-weibull distribution: A flexible parametric model for survival analysis*, Scandinavian Journal of Statistics 44 (2017), pp. 62–83.
- [11] L. Bottou, F.E. Curtis, and J. Nocedal, *Optimization methods for large-scale machine learning*, SIAM Review 60 (2018), pp. 223–311. Available at <https://doi.org/10.1137/16M1080173>.
- [12] B. Bradley and S. Taqqu Murad, *Financial risk and heavy tails*, Handbook of heavy tailed distributions in finance (2003), pp. 35–103.
- [13] B. C. and X.H. Z., *Non-homogeneous markov process models with informative observations with an application to alzheimer’s disease.*, Biometrical Journal 53 (2011), p. 444–463.
- [14] L.J.R. Esparza and F. Baltazar-Larios, *A stochastic expectation—maximisation (em) algorithm for construction of mortality tables*, Annals of Actuarial Science, 12 (2018), pp. 1–22.
- [15] B. Gompertz, *On the nature of the function expressive of the law of human mortality, and on a new mode of determining the value of life contingencies*, Philosophical Transactions of the Royal Society of London 115 (1825), pp. 513–583.
- [16] R.A. Hubbard, L.Y.T. Inoue, and J.R. Fann, *Modeling nonhomogeneous markov processes via time transformation*, Biometrics 64 (2008), pp. 843–850. Available at <http://www.jstor.org/stable/25502142>.
- [17] C.H. Jackson, *Multi-state models for panel data: The msm package for R*, Journal of Statistical Software 38 (2011), pp. 1–29. Available at <https://www.jstatsoft.org/v38/i08/>.
- [18] M. Neuts, *Probability distributions of phase type.*, In Liber Amicorum professor emeritus H. Florin (1975), p. 173–206.
- [19] P.Y. Nielsen, K.H. Andersen, and S. Hansen, *The gompertz law emerges naturally in systems of interacting failures*, Scientific Reports 14 (2024), p. 51669.
- [20] A. SLAVÍK, *Product Integration. Its History and Applications.*, Matfyzpress, Prague., 2007.
- [21] K. T. and G.J. McLachlan, *The EM Algorithm and Extensions.*, Wiley, 2008.
- [22] A. Tahira and M.Y. Danish, *A generalized gompertz promotion time cure model and its fitness to cancer data*, Heliyon 11 (2024), p. e32038. Available at <https://doi.org/10.1016/j.heliyon.2024.e32038>.
- [23] A.P. Zwart, *Queueing systems with heavy tails* (2001).